POLITECNICO
MILANO 1863

SCUOLA DI INGEGNERIA INDUSTRIALE
E DELL'INFORMAZIONE

Executive Summary of the Thesis

SmallSats Mars Aerocapture Optimal Guidance with Direct Force Control

Laurea Magistrale in Space Engineering - Ingegneria Spaziale

Author: Iñigo Prieto Boveda

Advisor: Prof. Michèle Roberta Lavagna

Co-advisor: Daniele Barberi Spirito

Academic year: 2022-2023

Acronyms

AutoNav Autonomous Optical Navigation.

DFC Direct Force Control.
DM Drag Modulation.
DSN Deep Space Network.

EDL Entry Descent and Landing.
ESPA EELV Secondary Payload Adapter.

FNPAG Fully Numerical Predictor-corrector Aerocapture Guidance.
FPA Flight Path Angle.

MSL Mars Science Laboratory.

NPC Numerical Predictor-Corrector.

OpNav Optical Navigation.

PICA Phenolic Impregnated Carbon Ablator.
PS Propulsion Subsystem.

TPS Thermal Protective System.

1. Introduction

SmallSat aerocapture has been mainly studied in literature by means of Drag Modulation (DM) and the use of drag increment devices such as drag skirts. The promising advantages that Direct Force Control (DFC) can provide and the higher technological readiness level of aeroshell capsule-like vehicles make its study applied to small satellites appealing. Since higher thermal and structural load constraints can be faced, aerocapture manoeuvre could be enabled.
This study will assess two main topics: the feasibility of the manoeuvre using the DFC with an aeroshell capsule respecting Smallsat form factor constraints and the development of an optimality-based aerocapture guidance scheme. A numerical simulation environment is developed and used to address the guidance method feasibility and enable the guidance algorithm development. Mathematical analysis has been employed to obtain the optimal control strategy.

2. Feasibility

2.1. Capsule Design and Constraints

A parametric design of the aeroshell capsules respecting the EELV Secondary Payload Adapter (ESPA) size and interface constraints has been conducted. To correctly address the trajectory's feasibility, a parametric capsule design has been performed exploiting hyperbolic contours

for their aerodynamic properties variations [7]. Vehicle constraints have been selected according to previous existing values for Mars Entry Descent and Landing (EDL) missions. From the aerodynamic study results, the limit angles to obtain an error lower than 10% when introducing one dimension assumption [1]. The minimum altitude trajectory constraint has been introduced because of Mars' sheer landscape and the high elevation of its mons, such as the Olympus mons. Vehicle and trajectory constraints are reported in Table 1.

Table 1: Vehicle and Trajectory Constraints

Property	Value
$\dot{Q}_{Max}$	1 [kW/cm^2]
q_{∞}^{Max}	16 [kPa]
n_{Max}	13 [g's]
h_{Min}	26.6 [km]
$\alpha_{Max/Min}$	±20 [deg]
$\beta_{Max/Min}$	±20 [deg]

2.2. Nominal Corridors

Nominal corridors have been computed covering the different problem parameter variations, considering the hyperbolic parameters 1.1, 1.15, 1.2, 1.3, 1.4, and 1.5 for the capsule design. From nominal corridors, the following conclusions have been extracted. Lower ballistic coefficients provide shallower trajectories, displacing the corridor upwards, which proves advantageous as an increase in the feasible region is obtained from milder load conditions encountered during the trajectory. Three factors can decrease the ballistic coefficient:

1. Reduce the vehicle's mass.
2. Increase the vehicle's reference surface.
3. Increase the vehicle's drag coefficient. (limited by aerodynamics).

The other main parameter related to the mission feasibility and the capability of the spacecraft to deal with trajectory uncertainty is the corridor width. The corridor width is more influenced by the L/D ratio of the vehicle, as shown from the capsule's parametric study. This fact goes against item 3. Because of the tight encountered corridors on Smallsat aeroshells at Mars, it would be preferable to opt for a greater L/D ratio while punishing trajectory loads, for which this kind of vehicle is better suited. The only free variable remaining for the mission designer would be making the spacecraft as lightweight as possible to encounter milder heat and structural loads.

Increasing the capsule's hyperbolic parameter increases the $S_{Ref}C_D$ figure while raising the L/D ratio too. Hence, shallower and wider corridors are obtained for higher values of the hyperbolic parameters, improving the applicability of the aerocapture trajectory for Smallsat aeroshell vehicles aerocapture at Mars for a higher number of target orbits and entry conditions. Therefore, a=1.5 capsule was selected for the study's test mission, as it provides higher flexibility to the achievable missions. Conversely, as aerocapture is mainly intended to raise the delivered payload mass fraction, the maximum allowable mass admitted from ESPA ring constraints has been introduced and set to be equal to 181 kilograms.

2.3. Feasible Region

Targeted atmospheric interface conditions and target orbit highly influence the in-plane aerocapture corridor. The maximum and minimum density profiles shrink the corridor's width, and the vehicle and trajectory constraints will limit some regions to be used in order to prevent a failure case, such as burnout, a crash against a mountain, or a structural failure. Consequently, *'Aerocapture Designer'* tool has been developed to compute the DFC feasible region for user-specified aerocapture parameters, enhancing the system study of aerocapture for future mission designers, allowing conservative performance studies on a user-based parameter selection and safety factors introduction.

The minimum corridor width could also prevent a certain corridor region from being feasible, as errors during the atmospheric interface targeting exist (for Mars aerocapture system study by NASA, 3σ value was established at ±0.3 [deg] on the flight path angle), and wider corridors relax the guidance requirements as they obtain improved manoeuvrability. As a result, a minimum corridor width of 1

degree has been considered and introduced as a constraint on the feasibility region computation.

Given the constraints reported on Table 1, and the capsule design with a=1.5 and a 181 [kg] mass, the feasibility region has been computed for two different target orbits. These two target orbits cover the two main applicable cases of aerocapture: low circular orbits with propulsive exoatmospheric manoeuvres and highly-elliptical target orbits for a later aerobraking manoeuvre.
From the reported results in Figure 1 and Figure 2, low circular target orbits are better suited for the small-satellite class missions exploiting DFC with aeroshell technology. In the high elliptical case, the lower entry velocities are prevented because of the encountered tight corridor width. In contrast, for higher ranges, the maximum dynamic pressure constraint keeps decreasing the feasible region until turning it unfeasible due to the reduced corridor width. Thus, only medium to high entry velocities could be used for high radius of apoapsis targeting. On the contrary, the low radius of apoapsis targeting orbits spans almost completely the whole range of incoming velocities for Mars aerocapture.

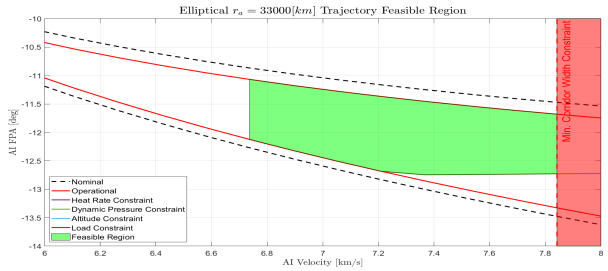

Figure 1: High radius of apoapsis targeting feasible region

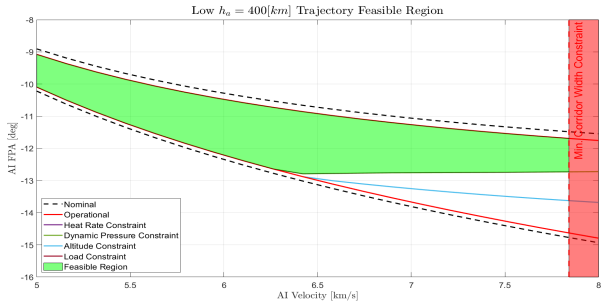

Figure 2: Low radius of apoapsis targeting feasible region

The out-of-plane manoeuvrability will depend on the trajectory. Higher capabilities have been found to be obtained when higher trajectory times of flight are encountered. For the worst-case conditions, the inclination variation over the incoming orbital plane achievable ranges from 7 to 13 degrees, depending on the target orbit and the arrival velocity.

3. Guidance

3.1. Optimal Control Problem

The weighted sum optimal functional considering the two main figures of merit influencing the aerocapture's manoeuvre system performance Optimal Control Problem (OCP) has been solved. The problem has been divided into two smaller sub-problems, exploiting the longitudinal and lateral channels decoupling provided by DFC. The longitudinal channel objective function solves for the in-plane exoatmospheric ΔV and total heat minimisation. In contrast, the lateral resolution solves the out-of-the-plane ΔV minimisation, which is equivalent to final inclination error minimisation for the circular orbit case.

The longitudinal channel resolution requires numerical methods. The problem has been transcripted into an NLP and solved through collocation methods. The mass and volumes required for the Thermal Protective System (TPS) and the Propulsion Subsystem (PS) have been computed for different weighting function values. Improvement is obtained in terms of mass and volume for the trajectories privileging ΔV minimising trajectories, considering Phenolic Impregnated Carbon Ablator (PICA) and hydrazine monopropellant. However, the change is small, and the control strategy reported for ΔV minimisation follows a single switch almost bang-bang full lift-up full lift-down strategy, similar to the one reported on [3]. This fact can be exploited as an advantage for the online guidance scheme implementation.

When a linear control law is assumed on the side-slip, the lateral channel's optimal control strategy can be obtained by applying the *Pontryagin's minimum principle*. The singular arc non-existence is achieved by proof of contradic-

tion with the maximum's principle, leading to a bang-bang optimal control strategy for the lateral channel.

3.2. Online Guidance

The control strategies obtained from the OCP resolution have been implemented into an online Numerical Predictor-Corrector (NPC) algorithm, which is adapted to deal with encountered day-of-flight uncertainty, following a similar strategy to the one suggested by [5] on the bank-angle modulated aerocapture guidance. Exploiting the fact of a single-switch bang-bang control strategy, the online algorithm can be divided into a multi-phase scheme, reducing the problem to three different phases: phase one, the transition phase, and phase two.

This implementation allows the predictor-corrector to solve for a *univariate parametric optimisation problem* on each guidance call, reducing the computational burden compared to predictive model controls. The control variable will depend on the guidance phase: the switch time during phase one and the constant aerodynamic angle till the end of the trajectory during phase two. The transition phase is implemented to skip the guidance call while the control switch is being performed so as to replicate the optimal control structure. The ΔV minimisation problem is solved by exploiting the *Golden-section Search* algorithm because a bounded optimisation is required to deal with the problem's discontinuities, as introduced by [4]. The longitudinal and lateral channels have been divided, so they can be parallelised, considering the small satellite's limited computational capabilities.

A first-order fade memory filter has been implemented to close the loop feedback with the real system and improve the guidance performance. Attitude kinematic constraints have been implemented on the velocity and acceleration constraints of the vehicle's actuators, as performed in [6]. To account for the limitation on small-satellite actuation, the cited study's considered values have been halved, leading to a rate limit of 1.25 [deg/s] and an acceleration limit of 0.5 [deg/s^2]. The onboard aerodynamic model is based on a linear piece-wise linearisation of MarsGram's mean profile, and the aerodynamic coefficients are based on one-dimensional polynomial regressions.

To prevent destructive trajectories, a reactive relief logic has been implemented to prevent maximum dynamic pressure and minimum altitude constraint violations, which happen to be the most restrictive constraints during the mission analysis phase.

3.2.1 Failure Preventing Measures

Within the longitudinal guidance logic, some infrequent convergence problems arose in the online optimisation, which led to failure cases. These were solved by a predictors estimation final logical state condition introduction, which successfully mitigated them.

Also, failure cases were encountered for the cases in which an overestimation of the orbital energy happened for introduced high uncertainty state estimation at the atmospheric interface. A higher robustness algorithm is obtained when the atmospheric state interface is set to the minimum energetic level at the cost of a performance decay.

3.3. Algorithm Validation

A comparison with the re-implemented guidance based on NASA's Fully Numerical Predictor-corrector Aerocapture Guidance (FNPAG) for DFC presented in [6] has been used for algorithms testing validation. Same entry conditions, atmospheric dispersions, and equivalent target orbits have been considered. Differences in the vehicle used and the entry flight path angle considering the mission's corridor exists. Results show the correct performance of the algorithm and lay within the average results reported, even in different mission scenarios, with different capsules, initial conditions and systematic errors considered.

3.4. Navigation Sensitivity Analysis

Only a few studies of aerocapture for small satellites on Mars navigation are found, in [2] entry dispersion correlated from Mars Science Laboratory (MSL) were employed. These are used as the baseline entry interface dispersions for the sensitivity analysis. The sensitivity analysis has

been performed by setting the same MarsGram density, winds and dust storm conditions, leading to a deterministic study scenario, taking the maximum values of dispersions and applying a varying multiplication factor. The target orbit is a 400 [km] circular orbit, with 80 [deg] inclination and an arrival state given in Table 2. The OCP reported a $\Delta V = 88.8[m/s]$ for this condition.

Table 2: Atmospheric Interface Conditions

Parameter	Value
h_{EI}	130 [km]
θ_{EI}	30 [deg]
ϕ_{EI}	0 [deg]
V_{EI}	6.1 [km/s]
$\overline{\gamma}_{EI}$	-12 [deg]
ψ_{EI}	10 [deg]

An almost linear worsening of the aerocapture guidance performance with the multiplication factor is obtained. This fact reduces the attractiveness of the aerocapture mission if posterior big propulsive manoeuvres are expected. Hence, two scenarios could be faced, greater uncertainty management with less sensitive atmospheric insertion for later atmospheric correction by aerobraking. Or more precise atmospheric entry target and navigation, with propulsive orbital corrections. These selections shall be system based considered as different trade-offs are introduced on the mission.

For the case where no uncertainty was found, a 110 [m/s] cost manoeuvre was obtained. This means that around a 25% worsening when compared to the ideal OCP solution is obtained, leading to a near-optimal performance of the online guidance when tested against the developed 'Real System' model.

3.5. Monte Carlo Results

To test the aerocapture performance and robustness, the exact same target mission considered in subsection 3.4 has been employed with the same initial conditions reported in Table 2. The considered dispersions are reported on Table 3, where the entry dispersions are based as previously on [2], with a 100% increase in the position-related components to produce a conservative analysis applied to the small-satellite navigation capabilities. This increment has been considered since compared with obtained dispersions during *LiciaCube* operation, much worse position-related components were found even if different performance is expected since it is planet-relative navigation.

Table 3: Atmospheric Interface Conditions

Variable	Maximum Dispersion
Initial Radius	uniform, σ=1.48 [km]
Initial Longitude	uniform, σ=0.024 [deg]
Initial Latitude	uniform, σ=0.034 [deg]
Initial FPA	uniform, σ=0.013 [deg]
Initial Azimuth	uniform,σ=0.0075 [deg]
Initial Velocity	uniform, σ=0.49 [m/s]
Mass	linear, $\dot{m}$=3/1500 [kg/s]
Bank Angle	systematic, 1 [deg]
Gram Seed	uniform, 1-29999
Gram Dust τ	uniform, 0.1-0.9
Aero Coefficients	systematic, 10%
Atm. Winds	MarsGram
Atm. Density	MarsGram
FPA target	uniform, $\sigma = \pm 0.3$ [deg]

Monte Carlo analysis with 100 sample cases with no failed trajectories is obtained. Worse performing results are obtained for higher entry flight path angles. The higher time of flight could explain the trend since for higher the trajectory time, the higher will be the error accumulation effect.

One out-layer is found on the ΔV results, and it can be a product of two main effects, the flight path angle and the navigation uncertainty. The combination of the high level of navigation uncertainty and high trajectory time of flight could explain the worst-behaving result. No correlation between guidance performance and dust storm intensity is found, and it can be concluded that the guidance is robust against them.

For the lateral channel case, most results lay

well-within 0.5 degrees, improving the performance for the increase in the value of the entry flight path angle. Three out layers can be found, which have not been able to tackle the atmospheric uncertainty during the trajectory. A lateral channel's logic misbehaviour can cause the out-layers, and further analysis would be required for its determination. The lateral guidance logic could be improved as performed on the longitudinal channel to prevent out-layer cases. However, due to the limited population, it has yet to be performed and has not been done in the current guidance implementation.

The statistical performance data of the analysis is reported on Table 4. Also, the reduced case delivery uncertainty has been considered since high variation with respect to the entry flight path angle has been observed—a 27% performance improvement over the full delivery dispersion is found on the 3σ value, reported on Table 5. The total manoeuvre cost is performed considering the periapsis raise, and the inclination correction manoeuvres are performed simultaneously.

Table 4: Monte Carlo Results Flight Path Angle (FPA)=[-12.3,-11.7][deg]

Manouvre	Mean	3σ
Periapsis Raise	87.5 [m/s]	106.5 [m/s]
Apoapsis Corr.	81.8 [m/s]	267.6 [m/s]
Inclination Corr.	13.5 [m/s]	62.9 [m/s]
Total	171.43 [m/s]	339.90 [m/s]

Table 5: Monte Carlo Results FPA=[-12.3,-12][deg]

Manouvre	Mean	3σ
Periapsis Raise	90.5 [m/s]	105.8 [m/s]
Apoapsis Corr.	56.2 [m/s]	166.7 [m/s]
Inclination Corr.	17 [m/s]	65.9 [m/s]
Total	149.39 [m/s]	248.26 [m/s]

3.6. Fully Propulsive Comparison

For the propulsive case, a hydrazine monopropellant-based system has been considered with an $I_{sp} = 230[s]$, and a 25% margin has been included to account for the tank and engine allocation. A total heat of 15 kJ/cm^2 for the total heat has been considered on the TPS sizing to account for a 10% margin with respect to the worst-case scenario. Small satellites' maximum mass and volume are considered from ESPA size constraints.

From obtained results reported in Table 6 and Table 7 report the great advantage of aerocapture compared to the fully propulsive case. This resulted in accomplishing a doable mission for the small satellite class aerocapture. Provided results can not be argued to extract the better achievable performance with the present guidance scheme since higher-level analysis shall be performed for the parameter tuning, which is not achieved in the present work due to computational and time limitations.

Table 6: 0.6[deg] FPA Dispersion Aerocapture vs Fully-Propulsive Capture

Property	Aerocap.	F-P	Benefit
ΔV[km/s]	0.34	2.65	87.17%
Mass[kg]	36.47	156.26	76.66%
Volume[m^3]	0.0494	0.1556	68.25%
Av. Mass	79.84%	13.66%	119.78 [kg]
Av. Vol.	88.20%	62.80%	0.106 [m^3]

Table 7: 0.3[deg] FPA Dispersion Aerocapture vs Fully-Propulsive Capture

Property	Aerocap.	F-P	Benefit
ΔV[km/s]	0.24	2.65	90.63%
Mass[kg]	28.42	156.26	81.81%
Volume[m^3]	0.0413	0.1556	72.36%
Av. Mass	84.30%	13.66%	127.84[kg]
Av. Vol.	90.12%	62.80%	0.114[m^3]

4. Conclusions

It can be concluded that aerocapture on Mars using DFC on an aeroshell capsule-like vehicle is feasible. The relaxation provided by the aeroshell capsule-kind compared to drag sail vehicles enables the aerocapture to be performed

on Mars. A correct capsule aerodynamic optimisation shall be performed to increment the L/D ratio so as to obtain enough corridor width for the vast range of arrival conditions and targeted orbits, even if low aerodynamic efficiency capsule shapes are employed.

The squeezing of the feasible region for the higher radius of apoapsis targeting leads to a better suit of the DFC on small satellites aeroshell capsule-like vehicles to low to medium target orbits. The non-jettisoning required during aerocapture allows its utilisation on later aerobraking manoeuvres, which can exploit the fact of deeper dives into the atmosphere to reduce the aerobraking manoeuvre time, taking advantage of the remaining TPS.

The guidance scheme shows robust behaviour when tested on the developed 'Real System' model developed, and high perturbation conditions are introduced, such as dust storms. From subsection 3.4, a near-optimal result can be obtained from the case of zero atmospheric interface uncertainty, corresponding to a 25% worsening on the overall ΔV. Hence, the guidance could be considered to provide great performance, finding a bottleneck in the atmospheric insertion uncertainty and on the online's navigation filter.

The main guidance bottleneck is found because navigation limitations provoked by the surrounding ionisation during atmospheric flight prevent the state updating during aerocapture. Since no state updates during the trajectory exist, the initial state error is propagated forward in the model and added to the model's existing error. Consequently, state drift arises as the trajectory time increases. This causes drastic performance issues, greatly impacted by the dispersions of the state knowledge at the atmospheric insertion, as reported in subsection 3.4.

As a consequence, navigation uncertainty reduction campaigns will be necessary previous to the atmospheric entry. Radiometric tracking from Deep Space Network (DSN) and Optical Navigation (OpNav) would be required to reduce the atmospheric entry state covariance. Autonomous Optical Navigation (AutoNav) could even improve the state estimation since measurements just before the hypersonic flight regime could be considered.

5. Acknowledgements

I would like to use this opportunity to convey my profound gratitude to Prof. Michèle Lavagna for allowing me to perform this research on the Aerocapture topic and for serving as my thesis advisor. Also, I want to convey my sincere gratitude to Daniele Barberi, my co-advisor, for his assistance, direction, and encouragement throughout the research process. His opinions and feedback have been really beneficial in forming the final thesis outcome.

Giovanni Zanotti and Jacopo Prinetto, PhD researchers at Politecnico di Milano, deserve my gratitude for their readiness to assist me during the research on Navigation and Optimal Control matters. Also, I wish to thank PhD David De La Torre Sangrà from UPC for sharing the MEMM engineering tool with me and giving me insightful recommendations regarding atmospheric modelling.

References

[1] Rohan G Deshmukh, David A Spencer, and Soumyo Dutta. Investigation of direct force control for aerocapture at neptune. *Acta Astronautica*, 175:375–386, 2020.

[2] G Falcone, JW Williams, and ZR Putnam. Assessment of aerocapture for orbit insertion of small satellites at mars. *Journal of Spacecraft and Rockets*, 56(6):1689–1703, 2019.

[3] Joshua K Geiser and Daniel A Matz. Optimal angle of attack control for aerocapture. In *AIAA SCITECH 2022 Forum*, page 0608, 2022.

[4] Jarret M Lafleur. The conditional equivalence of δv minimization and apoapsis targeting in numerical predictor-corrector aerocapture guidance. Technical report, 2011.

[5] Ping Lu, Christopher J Cerimele, Michael A Tigges, and Daniel A Matz. Optimal

aerocapture guidance. *Journal of Guidance, Control, and Dynamics*, 38(4):553–565, 2015.

[6] Daniel A Matz and Christopher Cerimele. Development of a numeric predictor-corrector aerocapture guidance for direct force control. page 0847. AIAA Scitech 2020 Forum, 2020.

[7] Hirotaka Otsu. Aerodynamic characteristics of re-entry capsules with hyperbolic contours. *Aerospace*, 8(10):287, 2021.